J. Fluid Mech. (1985), *vol.* 157, *pp.* 305–326
Printed in Great Britain

Characteristics of a trailing-edge flow with turbulent boundary-layer separation

By B. E. THOMPSON AND J. H. WHITELAW
Imperial College of Science and Technology, Department of Mechanical Engineering, Fluids Section, London SW7 2BX

(Received 23 May 1984 and in revised form 5 February 1985)

Experimental techniques, including flying-hot-wire anemometry, have been used to determine the pressure and velocity characteristics of a flow designed to simulate the trailing-edge region of an airfoil at high angle of attack. Emphasis is placed on the region of recirculating flow and on the downstream wake. It is shown that the effect of this recirculation is large even though the details of the flow within it may be unimportant. Normal stresses and cross-stream pressure gradients are important immediately upstream and downstream of the recirculating flow and are associated with strong streamline curvature. The relative importance of the terms in the transport equations for mean momentum and turbulence energy are quantified and the implications for procedures which solve potential-flow and boundary-layer equations and for alternative calculation methods are discussed.

1. Introduction

The development of high-lift wing configurations requires understanding of the flow in the vicinity of the trailing edge for configurations which include high angles of attack with consequent boundary-layer separation due to sustained adverse pressure gradient. The existence of boundary-layer separation, with its associated region of recirculating flow, poses a special problem for current design methods, as described for example by Cebeci, Stewartson & Whitelaw (1984), and these can only be overcome with improved knowledge based on experiments. The present investigation was undertaken to determine the more important aspects of a boundary-layer flow which separates on a trailing flap, the recirculating flow and the downstream wake. The results are presented in sufficient detail to show the main flow characteristics: further details necessary for the evaluation of design methods have been reported by Thompson (1984).

It is known that the interaction of solutions of potential and boundary-layer equations can be used to represent small regions of recirculation, see McDonald & Briley (1984), but that large regions of recirculation require the solution of transport equations involving two components of pressure gradient and turbulence diffusion. The present recirculating flow is of the second type and Adair, Thompson & Whitelaw (1984) have reported the results of preliminary calculations. It is hoped that these measured results will assist the development of calculation procedures.

The present flow simulates the trailing-edge region of an airfoil at high angle of attack, and involves a larger region of separated flow than previous related investigations such as those of Viswanath & Brown (1983) and Nakayama (1984). Emphasis is placed on the characteristics of the recirculation region and its influence on the downstream wake as its larger dimensions have allowed results to be obtained in greater detail and possibly with improved accuracy.

Conventional pressure probes and a hot-wire anemometer have been used to determine velocity characteristics except in the region of recirculating flow where a flying-hot-wire arrangement was used. Coles & Wadcock (1979) have also used flying-hot-wire anemometry to take measurements in the recirculating flow near the trailing edge of an airfoil whereas laser velocimetry has been preferred by Simpson, Chew & Sivaprasad (1981), Viswanath & Brown (1983) and Nakayama (1984).

The flow configuration and measurement techniques are described in the following section. The results are presented in §§3 and 4, which deal respectively with mean and turbulence characteristics, and are discussed in §5.

2. Flow configuration and measurement techniques

A 1035 mm flat plate with a trailing flap was located in the working section of a low-speed wind tunnel as shown in figure 1. The flat plate was set at an angle of 1° and the flap at 17.5°, both with respect to tunnel coordinates, after preliminary experiments to determine the angles which gave rise to the required region of separated flow on the flap. The boundary layers on the tunnel walls and upper surface of the plate were tripped by 1.5 mm diameter wires located at the start of the flat plate which corresponds to the exit of the 8 to 1 contraction. The trailing flap was 249 mm long and was connected to the flat plate by a radius of 812.5 mm. This arrangement caused the upper-surface boundary layer to separate 187 mm from the trailing edge and gave rise to the characteristic boundaries indicated on figure 1.

In the upstream region of the upper and lower surfaces and for most of the wake, the flow had a preferred direction and comparatively low turbulence intensities so that it was possible to measure mean values of pressure and velocity with impact probes and the velocity characteristics with a stationary-hot-wire anemometer. Close to separation and where the flow angle deviated from that near the surface of the flap, tunnel roof or floor, a five-tube pressure probe was used to quantify the flow angle, velocity and static pressure. Close to the wall a flattened Pitot tube allowed measurements of mean velocity with reduced blockage and gradient effects.

Flying-hot-wire anemometry was used in regions where flow reversals occurred. It required a hot-wire probe to travel through the flow at a known velocity of sufficient magnitude to avoid the signal rectification associated with the use of a stationary hot wire in flows with negative velocities. The flying-wire arrangement of Thompson & Whitelaw (1984) was used here and allowed the measurement of the magnitude and direction of mean velocity and the corresponding Reynolds stresses in the region of recirculating flow.

Details of the measurement methods are not included so as to allow for emphasis on the results and related discussion. It should be noted, however, that three types of pressure probe and two hot-wire arrangements were involved and were complemented by measurements of wall static pressure and flow visualization. The dimensions of the Pitot tube used away from the separated flow were 0.82 and 1.24 mm inside and outside diameters, respectively, and those of the flattened-end Pitot tube were 0.31 and 1.33 mm inside and 0.48 and 2.11 mm outside. A five-tube probe of maximum cross-stream dimension 2.58 mm with five tubes of diameter 0.82 mm outside and 0.51 mm inside, was used to determine local flow angle and static pressure. Straight-wire (DISA 55P10), angle-wire (DISA 55P11) and cross-wire (DISA 55P61) probes were operated with constant-temperature anemometers (DISA 55M01/M10) and the instantaneous voltages recorded digitally by computer prior to analysis. Calibration was performed in the free stream of the wind tunnel and the

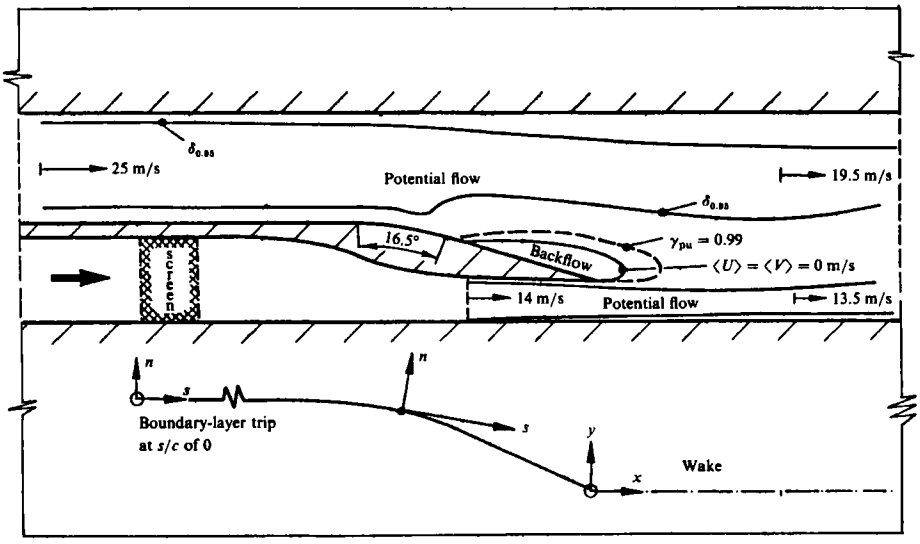

FIGURE 1. Flow configuration.

resulting linearization stored in the computer. The same approach was used with the flying hot wires with the additional information of wire position, trajectory, and speed known from geometry and a shaft encoder. The flow velocity characteristics were evaluated within the computer after subtracting the effect of probe motion. Measurement accuracy has been considered in detail by Thompson (1984) and, for present purposes, it is sufficient to note that none of the deductions are influenced by experimental error.

The two-dimensionality of the mean flow was established by flow visualization, wall-pressure and local-velocity measurements. Passive flow-control vanes were used to reduce the growth of secondary flows which occur in the corner of the boundary layer over the curved surface and flap, and were adjusted to maximize the extent over which the recirculation region was two-dimensional.

Visualization of the surface flow by means of a mixture of oil and titanium oxide particles showed that the boundary-layer flow over the flat plate was two-dimensional except within 30 mm of the sidewalls. This was confirmed by measurements of the near-wall flow with Preston and flattened Pitot tubes, which showed variations of less than 1 % over this 390 mm, and by measurements of wall pressure, mean velocity and Reynolds stresses which were within experimental error over more than 90 % of the tunnel width. The mean-separation line appeared straight and normal to the flow over the central 160 mm of the flap and a combination of hot-wire and flying-wire measurements confirmed that the two-dimensional region narrowed as separation was approached. Profiles of mean velocity at the location of mean-streamline detachment agreed within 1 % of the local values over the central 140 mm (31 %) of the tunnel width. The flying wire was also used inside the recirculation region to obtain velocity characteristics on the centreline and at 70 mm to either side and mean-velocity values agreed within 1.5 %.

Terms in the momentum-integral equation for two-dimensional subsonic flow with significant normal pressure gradient were evaluated using second-order-accurate methods for the integrals and derivatives and using the logarithmic law of the wall for the skin friction and velocity variation near the wall. The balance was within 6 %

$1+x/c$	U_e (m/s)‡	$\delta_{0.995}$ (mm)	δ_1 (mm)	δ_2 (mm)	H (mm)	$C_{P_{wall}}$
			Tunnel roof			
0.370	25.54	2.83	3.83	2.88	1.33	0.1106
0.650	24.97	3.71	6.07	4.25	1.42	0.1604
0.700	24.89	4.01	7.32	5.08	1.44	0.1846
0.750	24.20	4.31	8.43	5.49	1.53	0.2149
0.800	24.00	4.62	8.45	5.51	1.53	0.2410
0.850	22.98	4.71	9.16	5.70	1.61	0.3121
0.900	21.70	4.81	9.73	6.16	1.58	0.3524
0.950	20.97	4.97	12.02	7.19	1.67	0.3903
1.00†	20.27	5.18	13.53	7.81	1.73	0.4093
1.066	19.71	5.26	13.21	7.95	1.66	0.4330
1.099	19.70	5.66	13.08	8.04	1.62	0.4495
1.181	19.68	5.76	13.20	7.98	1.65	0.4638
1.230	19.33	6.18	13.86	9.24	1.50	0.4697
1.329	19.30	6.31	13.74	9.15	1.50	0.4827
			Tunnel floor			
1.033	13.86	3.31	2.61	1.94	1.34	0.4199
1.066	13.61	3.36	2.62	1.94	1.35	0.4321
1.099	13.42	3.39	2.65	1.95	1.36	0.4502
1.181	13.30	3.40	2.75	1.99	1.38	0.4640
1.230	13.28	3.71	2.96	2.14	1.39	0.4721
1.329	13.24	4.14	3.59	2.51	1.43	0.4820

† Plane of trailing edge.
‡ Free-stream velocity at $y = \delta$.

TABLE 1. Development of free-stream velocities and of roof and floor boundary layers

of the largest term in the regions of the upstream boundary layer approaching separation and the wake, including locations which were 50 mm away from the centreline. The largest discrepancies occurred in the immediate vicinity of mean-streamline detachment and just downstream of the trailing edge and this may be attributed largely to variations in the static pressure caused by flow-curvature effects associated with separation.

Cross-stream profiles of $\langle u^2 \rangle$, $\langle v^2 \rangle$ and $\langle uv \rangle$ obtained with stationary hot wires agreed, within the estimates of experimental errors of 3%, 10% and 4%, over the central 85% of the tunnel width in the upstream boundary layer, over the central 165 mm above the location of mean-streamline detachment, i.e. without flow reversals, and over the central 150 mm downstream of x/c equal to 0.2 in the wake. The values of $\langle u^2 \rangle$ obtained with the flying wire in the recirculating flow agreed within 3% across the flow over the central 130 mm of the tunnel width.

The measurements described in the following sections were obtained with a chord Reynolds number of 2.62×10^6 and results are presented in terms of a chord length based on the distance from the trip wire along the upper surface to the trailing edge of the flap, i.e. 1.518 m, and the reference velocity of 26.3 m/s. For reference purposes, the growth of the boundary layer on the floor and roof of the wind tunnel, and the variations of the free-stream velocities, are given in table 1.

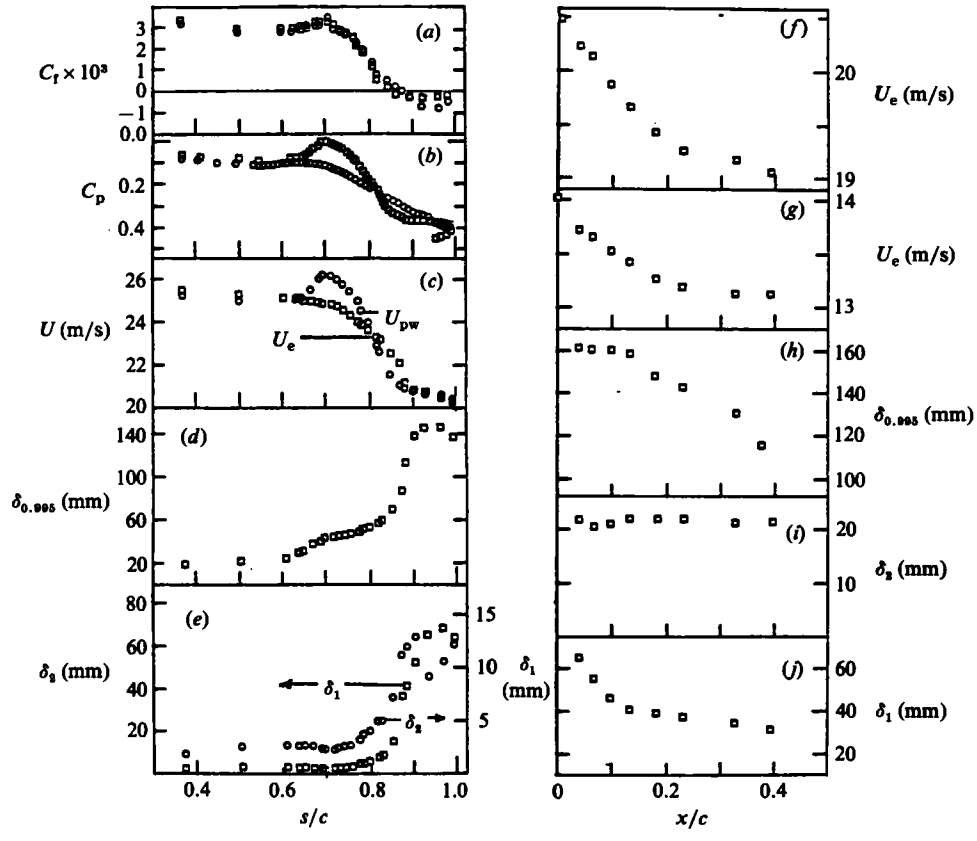

FIGURE 2. Parameters of mean-flow development. (*a*) Skin-friction coefficient: □, from Clauser chart; ○, estimated from Reynolds shear-stress distribution. (*b*) Static-pressure coefficient: □, surface; ○, at $n = \delta$ on the suction side. (*c*) Mean velocity on the suction side: □, at $n = \delta$; potential velocity at the wall (obtained using equation (1)). (*d*) Boundary-layer thickness corresponding to $U/U_e = 0.995$. (*e*) Integral thicknesses: □, δ_1 displacement thickness (left-hand scale); ○, δ_2 momentum thickness (right-hand scale). (*f*) Mean velocity at $y = \delta$ on the suction side. (*g*) Mean velocity at $y = \delta$ on the pressure side. (*h*) Boundary-layer thickness corresponding to $U/U_e = 0.995$ across the wake. (*i*) Momentum thickness. (*j*) Displacement thickness.

3. Mean-flow results

The skin-friction coefficient, wall static-pressure coefficient, growth parameters and free-stream values of pressure and velocity are shown on figure 2. The skin friction is zero at the location of mean streamline detachment, which can be deduced to have occurred at s/c of 0.879 where the boundary-layer thickness was about 75 mm, although intermittent back flow was measured some 40–45 mm upstream of this location. The influence of the change in wall curvature at s/c of 0.68 can be seen to have affected the pressure and velocity fields some 5% of chord further upstream. The static-pressure coefficients obtained at the wall and at the edge of the boundary layer indicate a cross-stream variation in pressure which occurs from just upstream of the curved section through to the trailing edge. The influence of separation can be seen where the suction-side wall-pressure distribution attains an almost constant value. Pressure recovery on the wall begins near the most upstream location of intermittent backflow and the streamwise pressure gradient along the wall is very small from here downstream to the trailing edge.

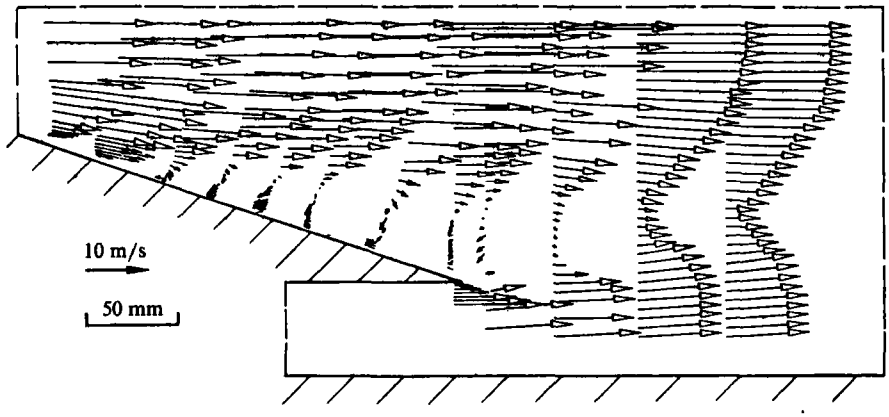

FIGURE 3. Vectors representing mean velocities in the vicinity of recirculation.

The boundary layer grows rapidly as separation is approached with the displacement and momentum thickness δ_1 and δ_2 attaining values at detachment of approximately 22 mm and 8 mm respectively. Values of the boundary-layer-thickness parameters have limited applicability around the recirculation region since terms in the cross-stream momentum equation are significant from upstream of detachment through the separated flow and into the wake. The distributions of the free-stream velocities (see also table 1) are shown and that on the suction side is larger, with the consequence that velocity gradients are smaller on the pressure side downstream of the trailing edge. The magnitude of the cross-stream pressure gradient increases as detachment is approached and at s/c of 0.826 achieves a value which is approximately 2.6 times that of the longitudinal pressure gradient. The implications of this result are discussed in §5.

The general organization of the mean velocities in the separated region is represented by the vectors of figure 3. The region of backflow is apparent near the trailing edge as are the pressure-side and suction-side shear layers, whose characteristics are important to the overall flow structure.

Profiles of stream-wise and crossflow mean velocity are shown on figures 4 and 5 respectively for the region up to separation, in the recirculating flow, and in the wake. It should be noted that the coordinate system has changed at the trailing edge to correspond to tunnel rather than to the surface coordinates used in the boundary layer. It can be seen that the cross-stream velocity in the separated region is generally larger than the corresponding streamwise-velocity component, particularly in the regions where the boundary layer that develops within the reversed-flow region separates and attaches to the surface, but is small compared with the free-stream velocity. Further, the negative-flow region extends about 25 mm beyond the trailing edge, after which the shear layers around the recirculation region interact and develop into an asymmetric wake. The measurements with a predominant downstream direction in the wake begin at x/c of 0.016 although here instantaneous flow reversals were still experienced. The intervening region features the suction-side recirculation bubble with its maximum 40 mm width and 210 mm length and negative mean velocities less than 11 % of the free-stream value. The free shear layer, which circumvents the upper boundary of the recirculation region, begins to form approximately 7 % of chord upstream of the location where the mean streamlines detach from the suction-side surface. In the velocity profiles downstream of this and before

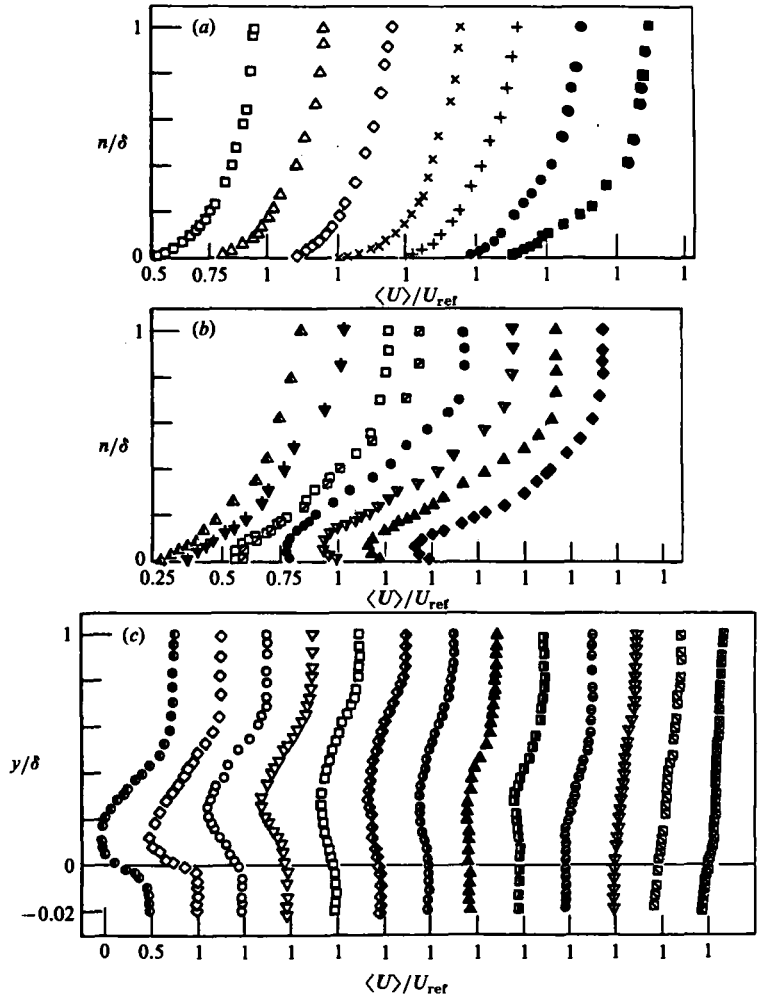

FIGURE 4. Distribution of streamwise mean velocity. (*a*) □, $s/c = 0.649$; △, 0.668; ◇, 0.695; ×, 0.718; +, 0.757; ●, 0.777; ■, 0.798. (*b*) ▲, $s/c = 0.826$; ▼, 0.852; □, 0.866; ▨, 0.886; ●, 0.905; ▼, 0.932; ▲, 0.968; ◆, 0.994. (*c*) ◐, $x/c = 0.006$; ◇, 0.050; ○, 0.066; ▽, 0.099; □, 0.132, ◈, 0.181; ◑, 0.231; ▲, 0.329; ◨, 0.428; ⊖, 0.494; ▽, 0.659; ▧, 0.988; ⊠, 1.153.

detachment, the mean-velocity gradient across the flow, $\partial U/\partial n$, decreases and then increases at a distance less than 10% of the boundary-layer thickness away from the wall. This corresponds to an inflection in the velocity distribution which occurs because the mean flow near the wall is deflected outwards around the region of recirculation. It is also associated with a maximum in the turbulent-shear-stress profiles and with an increase in normal stress production, as discussed in the following section, and eventually becomes the location of zero mean velocity. The velocity distributions in the separated region are characterized by the shear layer at the outer edge of the recirculation bubble and by the reverse-flow boundary layer which begins around the trailing edge and continues towards the location of mean-streamline detachment.

The near-wall flow over the upper surface is represented by the conventional law of the wall in the region prior to separation as reported by Thompson & Whitelaw

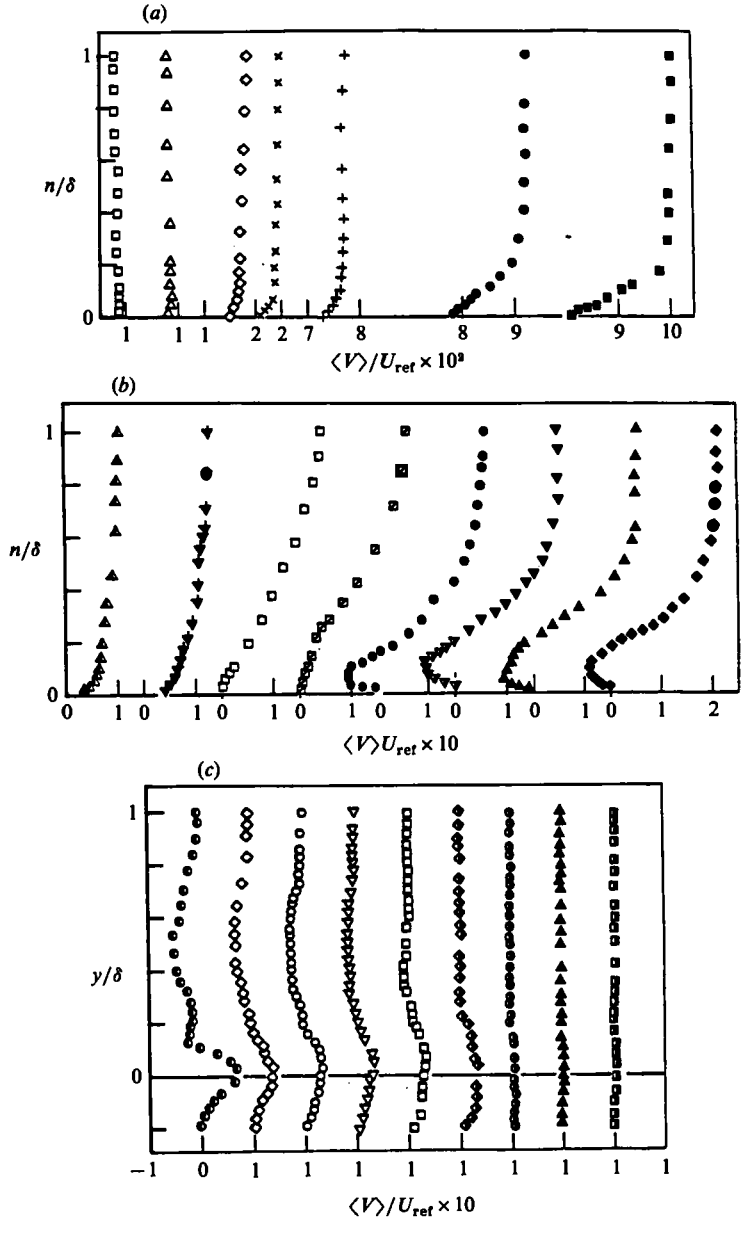

FIGURE 5. Distribution of crossflow mean velocity. (Symbols are shown on figure 4.)

(1982). The maximum height of the logarithmic region decreases from $Y+$ of about 700 on the upstream plate to $Y+$ of less than 30 at incipient detachment. The near-wall flow from upstream of separation through the backflow to the trailing edge is depicted on figure 6 with the closest measurement point at about 0.25 mm from the wall. The region of backflow is apparent and its cross-stream dimension increases from its inception at s/c of 0.879 until it extends over about 22 % of the boundary layer at the trailing edge. A log–linear velocity distribution also exists in the central backflow between Reynolds numbers of 600–9000, based on the perpendicular

distance from the wall and the free-stream velocity. Near the trailing edge where the backflow boundary layer starts to form and in the immediate vicinity of its detachment, the slope of the log-linear distribution changes with position along the surface and its outer limit is reduced to a minimum value of Reynolds number based on distance from the surface of about 2000.

The standard law of the wall with constants κ and B of 0.41 and 5.0, respectively, are represented by the Clauser lines drawn on figure 6, and it is apparent that this law is not appropriate downstream of the location of incipient detachment and in the backflow region. There does seem to be a a log-linear variation in the mean-velocity distributions across the reversed boundary layer but the values of skin-friction coefficient based on the standard log law are an order of magnitude smaller than those obtained by extrapolating the Reynolds shear stress to the wall. With values of c_f based on extrapolation of the local turbulent shear stress, a logarithmic law of the wall can be found to represent the near-wall mean-velocity profiles in the separated region but with log-law constants which change gradually from the standard values that are appropriate upstream of detachment to values of κ of 1.85 and B of 0.77 which fit the measured velocity distributions downstream of x/c of 0.90.

The measurements of Simpson *et al.* (1981) and Hastings & Moreton (1982) also show a log-linear region and, in a similar manner, their results do not seem to fit the standard law of the wall. It is also worth noting that the suggestion of Simpson (1983) to express the reversed mean-velocity profile as a function of the maximum negative velocity and its distance from the wall, does not describe the present results in the vicinity of detachment. In the central, fully developed region of the backflow from s/c of 0.93–0.98, the reversed-flow-velocity distributions are described by Simpson's function within the bounds of uncertainty imposed by the measurement of the location of maximum reverse velocity and its magnitude.

The very near wake, in which negative velocities occur, extends from the trailing edge to about x/c of 0.07 and encompasses about 12 % of the length of the recirculation bubble. The region of reversed mean flow decreases in width until it is no longer evident downstream of x/c of 0.021. In this reversed-flow region of the wake, mean velocities are less than 10 % of the suction-side free-stream velocity and the cross-stream-velocity component is as much as 1.5 times the maximum streamwise component.

The attached pressure-side boundary layer enters from beneath the trailing edge, where it has a thickness of 4 mm and a logarithmic region with a skin-friction coefficient of 0.0035. A second smaller region of recirculating flow, rotating in the opposite direction to the main recirculation bubble, is apparent in figure 3 immediately downstream of the trailing edge and between the pressure- and suction-side shear layers and balances the vorticity-transport equation in association with the beginning of the shear-layer interaction. This counter-rotating vortex has a cross-stream dimension less than one third that of the backflow and occurs as a consequence of the introduction of high-momentum flow from the pressure side beneath the low-momentum fluid of the backflow. Its occurrence is consistent with the observation that the pressure-side shear layer entrains fluid from the backflow for about the first 18 mm downstream of the trailing edge and, from here to the rear stagnation point, appears to supply fluid to the backflow.

The near wake begins downstream of where the pressure- and suction-side shear layers interact directly. In this region the shape factor asymptotically approaches 1.0, which was also found by Hah & Lakshminarayana (1982), as the displacement thickness increases with almost constant momentum thickness. Here, the mean flow

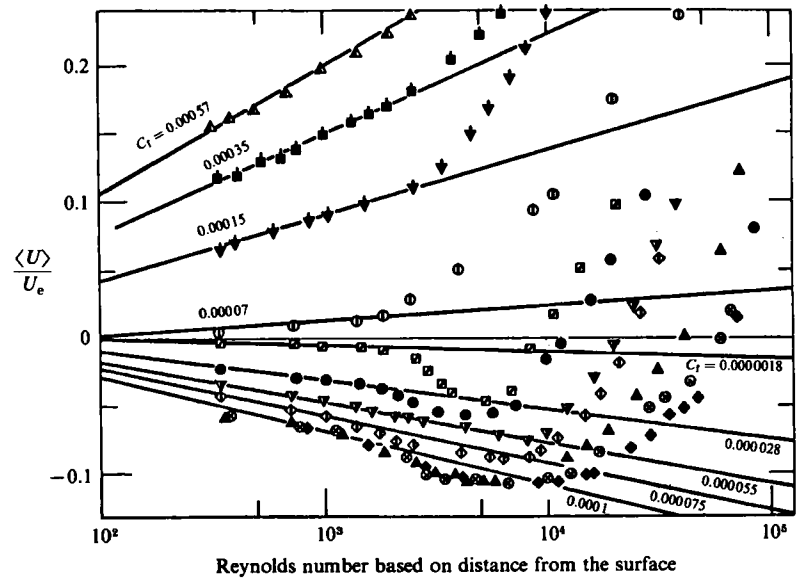

FIGURE 6. Clauser chart of near-wall mean velocities in the vicinity of the backflow. Clauser lines obtained with $\kappa = 0.41$; $B = 5.0$ (Symbols are as on figure 4(*b*) with the following additions: ■, $s/c = 0.839$; ⓘ, 0.874; ▽, 0.932; ◈, 0.955; ⊗, 0.980.

is in the positive X-direction and the cross-stream dimension of the region with instantaneous flow reversals diminishes until reversals are no longer apparent downstream of x/c of 0.07. The static-pressure variation also decreases with downstream distance and, beyond x/c of 0.066, the difference in static pressure between the suction and pressure side is gradually reducing and becomes negligible at about 20% of chord downstream of the trailing edge. Over this region the distribution of static pressure changes from a double-peaked profile apparent upstream of x/c of 0.15 to a single-peaked profile as a result of interaction of the upper- and lower-side shear layers. The mean velocity also recovers here with its minimum value increasing by about 2.8 times between x/c of 0.066 and 0.25 and the maximum gradient of mean velocity decreasing by about 33%.

In the far wake, beyond x/c of 0.25, the mean velocity recovers to a plane mixing layer. The profiles of mean velocity no longer have a distinct minimum and the static pressure is constant across the flow in the region downstream of 40% of chord from the trailing edge.

4. Turbulence results

The Reynolds stresses of figure 7 were measured from the trip wire downstream to separation and at distances greater than 1.5 mm from the wall. Upstream of s/c of 0.60, where the effects of surface curvature are noticeable, the Reynolds stresses agree well with those of Klebanoff (1954). Over the curved surface, the Reynolds stresses decrease through the boundary layer owing to the stabilizing effect of streamwise curvature, and non-dimensional values obtained using the wall potential velocity are in the range between those of Hoffman & Bradshaw (1978) and So & Mellor (1973). Their results were obtained in curved ducts with constant radii of curvature and with curvature parameters δ/R of 0.01 and 0.18, respectively, which

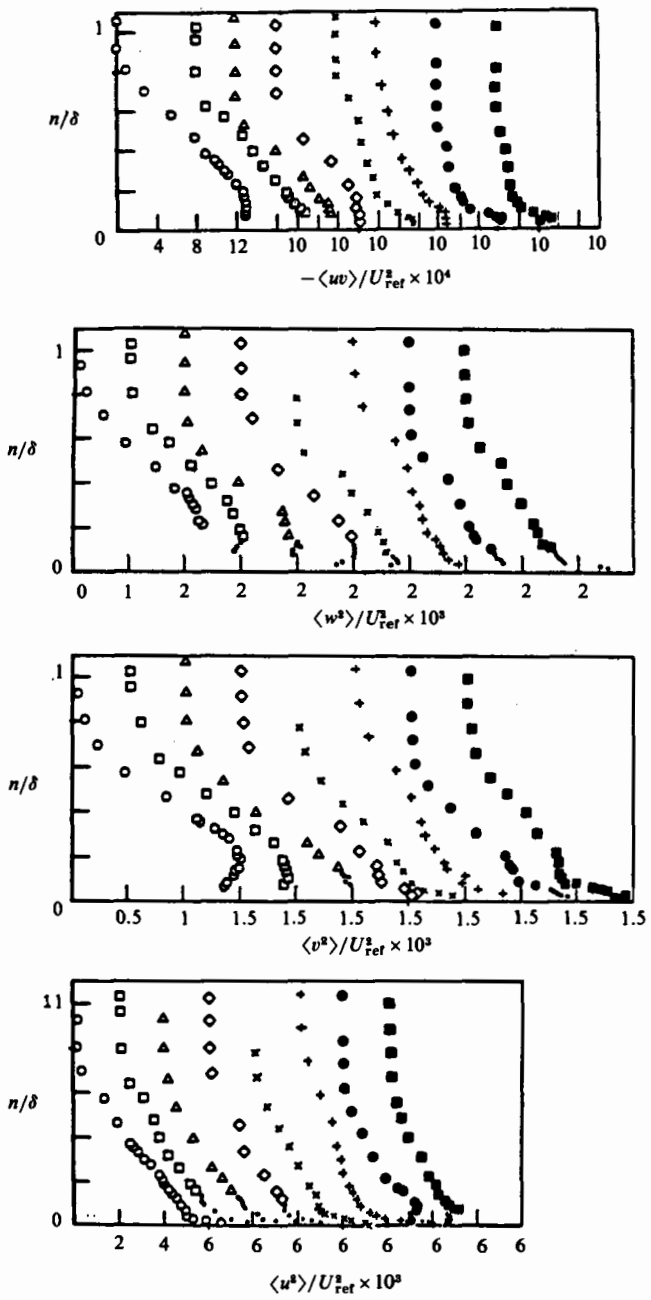

FIGURE 7. Distribution of Reynolds stresses in the region approaching separation. (Symbols are as on figure 4(*a*) with the additional profile at $s/c = 0.372$, ○).

bound the present value of 0.03. The recent measurements of Gillis & Johnston (1983) correspond to values of δ/R of 0.05 and 0.10 and are also consistent with the present values. The tunnel roof is not curved in the present configuration and this results in variations in the flow direction and static pressure through the boundary layer which preclude exact comparison with curved-duct flows. The main consequence of

this difference appears in the outer part of the boundary layer, where the turbulence intensities are higher than would be expected in curved-duct flow and the cross-stream variation of Reynolds stresses is more gradual. Curvature effects are comparable close to the wall and the present distributions of the Reynolds stresses are in good agreement with those in curved ducts prior to the region where the influence of separation is apparent. In this upstream region, the turbulence intensities scale with the potential velocity on the wall, i.e.

$$U_{\mathrm{pw}} = \left\{\frac{2(P_{\mathrm{T}} - P_{\mathrm{w}})}{\rho}\right\}^{\frac{1}{2}}, \tag{1}$$

where P_{T} refers to the total pressure in the free stream and P_{w} is the static pressure at the wall. In the region between the wall and about 65 % of the boundary-layer thickness, turbulence levels decrease with downstream distance: $\langle v^2\rangle^{\frac{1}{2}}$ is affected most and decreases by up to 50 % of its value at the start of curvature. The values of $\langle w^2\rangle^{\frac{1}{2}}$ decrease almost uniformly with downstream distance but at a rate of about 4 % cm^{-1} faster than the wall potential velocity. The Reynolds shear stress is constant for values of n/δ less than 0.2, varies linearly across the central part of the boundary layer and becomes negligible at a distance of about 80 % of the boundary-layer thickness from the wall.

The influence of separation is apparent downstream of s/c of 0.75 although instantaneous flow reversals are not in evidence here and mean-streamline detachment does not occur until s/c of 0.879. In this region between s/c of 0.75 and 0.879, the turbulence intensities increase close to the wall, i.e. below n/δ of about 0.5, as a result of extra production and locally decreased effects of stabilizing curvature. The largest effect is again observed in $\langle v^2\rangle^{\frac{1}{2}}$, whose maximum value moves away from the surface and increases by 25 % relative to the almost constant value of wall potential velocity found here and throughout the backflow. The Reynolds shear-stress distributions of figure 8 show a maximum value here which increases and moves progressively outwards as separation is approached. This is an indication of the development of the shear layer associated with the streamline that divides the forward and reversed flow. Above n/δ of 0.5, the effects of stabilizing curvature are similar to those further upstream and the normal stresses continue to decrease at approximately the same rate with downstream distances: they no longer correlate with the near-wall flow. All of the Reynolds stresses are suppressed to their free-stream value beyond about 75 % of the boundary-layer thickness because of curvature effects.

The probability of the occurrence of positive velocities is shown on figure 9 in the form of cross-stream profiles. Instantaneous flow reversals are detected close to the wall downstream of s/c of 0.845 and gradually spread outwards across the boundary layer until at s/c of 0.95 they occur over the inner 47 mm (35 %) of the boundary layer. Throughout this region the local turbulence intensity, $\langle u^2\rangle^{\frac{1}{2}}/\langle U\rangle$, exceeds 0.3. Positive instantaneous velocities were measured for at least some of the time at all locations: the smallest probabilities of downstream flow of about 0.02 were measured approximately halfway between the wall and the location of maximum values of reverse mean velocity. In the boundary layer and wake, the outer extremities of flow reversals coincided with the location of maximum Reynolds shear stress and the location of minimum values of γ_{pu} and $-\langle uv\rangle$ were also coincident. This indicates that the instantaneous reversed flow makes a positive contribution to the turbulence shear stress and does so at a rate proportional to the probability of backflow, which is not a direct function of the local mean-velocity gradient. As a consequence eddy-viscosity assumptions may be inappropriate in regions with flow reversals or at least where the probability of reversed velocity is large.

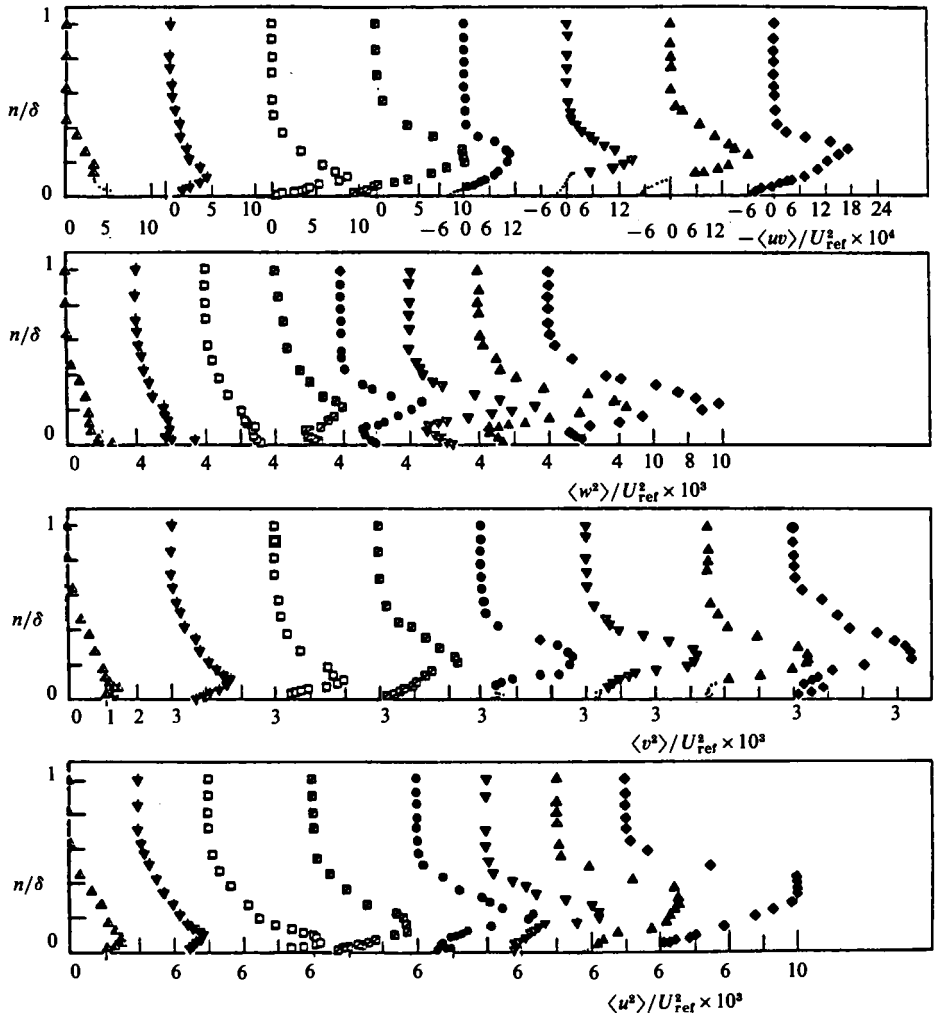

FIGURE 8. Distribution of Reynolds stresses in the vicinity of recirculating flow. (Symbols are shown on figure 4(*b*).)

In the backflow region, instantaneous flow reversals extend about 2.1 times further from the wall than the outer extremity of reversed velocity. The turbulence shear stress is constant over the inner 3 % of the boundary layer downstream of s/c equal to 0.96. Between the location of detachment and this point, an inner region of constant $\langle uv \rangle$ was not detected although it is likely to exist within 2 mm of the wall corresponding to the extent of the log-law region. Farther from the wall, the distributions of Reynolds shear stress show linear increases from the positive near-wall value to a negative maximum located at about n/δ of 0.25. The positive and negative magnitudes of $\langle uv \rangle$ increase gradually with distance along the surface over the inner part of the boundary layer and with the value at the negative maximum increasing by about 4 times over the length of the backflow region to about -1.5 m^2/s^2. The locations of the zero value of $\langle uv \rangle$ in the inner region correspond to the minima in the mean-velocity distributions and move gradually away from the wall in the backflow region. In the outer part of the boundary layer the turbulent shear stress remains suppressed due to the effects of streamwise curvature and is negligible outside of n/δ of 0.6.

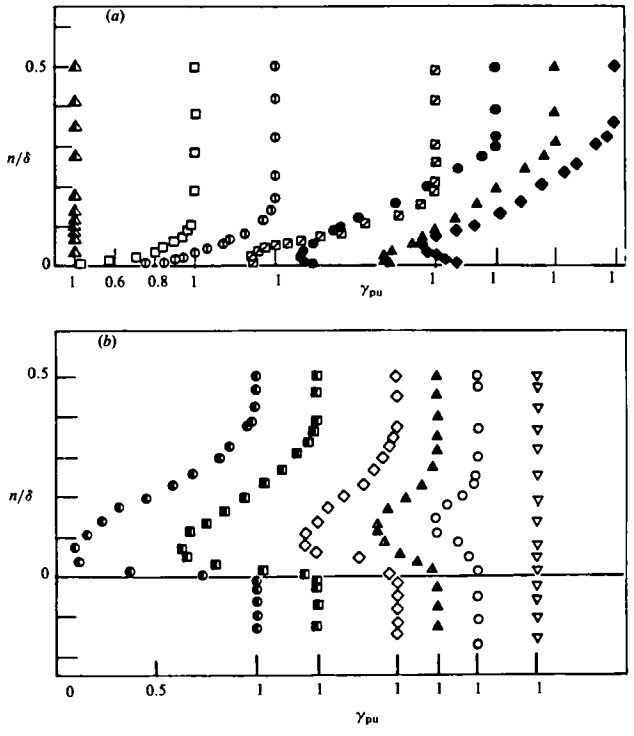

FIGURE 9. Probability of positive velocity. (Symbols for (*a*) are as on figure 6 and for (*b*) figure 4(*c*) with the following additions: ◨, $x/c = 0.028$ and ◭, 0.058.)

The profiles of the normal stresses downstream of s/c equal to 0.86 show two maxima which correspond approximately with the locations of inflections in the mean-velocity profiles. The inner maximum occurs at n/δ of 0.025 and the larger outer maximum appears at around 0.25 except in the region near detachment, where it is slightly closer to the wall at s/c of 0.15. The distributions of $\langle u^2 \rangle$ and $\langle v^2 \rangle$ are similar across the outer part of the boundary layer although $\langle v^2 \rangle$ is about 45 % of $\langle u^2 \rangle$. The outer maxima increases from 2.6 to 5.5 m^2/s^2 for $\langle u^2 \rangle$ and from 1.2 to 2.5 m^2/s^2 for $\langle v^2 \rangle$ over the backflow region and the location of these maxima corresponds to that of the negative maxima of turbulent shear stress associated with the dividing streamline around the recirculating region. In the very-near-wall region, the values of $\langle v^2 \rangle$ are less than 15 % of $\langle u^2 \rangle$ and $\langle w^2 \rangle$, and have a maximum value that decreases from 0.7 m^2/s^2 near detachment to 0.23 m^2/s^2 within the reversed-flow boundary layer. The distributions of $\langle u^2 \rangle$ and $\langle w^2 \rangle$ are almost identical across the outer 85 % of the boundary layer, where their values agree within 5 % of each other. Closer to the wall $\langle u^2 \rangle$ is generally larger although they are almost equal at the inner maxima. The cross-stream variation of $\langle w^2 \rangle$ in the near-wall region is greater than that of $\langle u^2 \rangle$ and is similar to that of $\langle v^2 \rangle$ in that the inner peak is pronounced.

In the reversed-flow boundary layer from s/c of 0.9 just downstream of detachment to the trailing edge, the profiles and levels of the turbulent normal stresses do not change and are approximately related by the ratios:

$$\langle u^2 \rangle^{\frac{1}{2}} = 2.40 \langle v^2 \rangle^{\frac{1}{2}}; \tag{2}$$

$$\langle u^2 \rangle^{\frac{1}{2}} = 1.02 \langle w^2 \rangle^{\frac{1}{2}}; \tag{3}$$

$$\langle v^2 \rangle^{\frac{1}{2}} = 0.43 \langle w^2 \rangle^{\frac{1}{2}}; \tag{4}$$

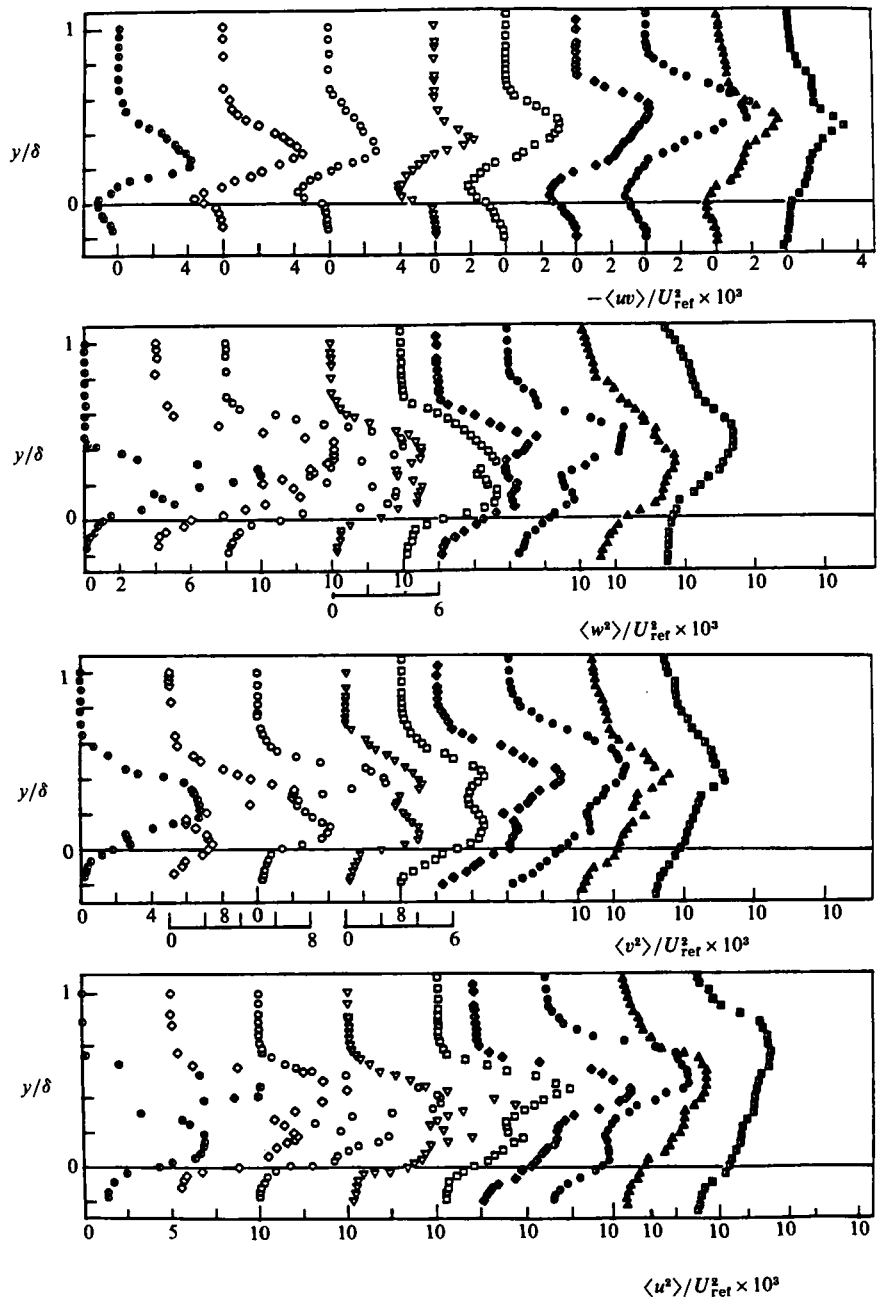

FIGURE 10. Distribution of Reynolds stresses in the very near and near wake. (Symbols are as on figure 4(*c*).)

with maximum values of 1.55, 0.27 and 1.48 m^2/s^2 for $\langle u^2\rangle$, $\langle v^2\rangle$ and $\langle w^2\rangle$ respectively in the backflow boundary layer.

The distributions of Reynolds stresses in the wake are shown in tunnel coordinates on figures 10 and 11. The turbulence structure of the wake is affected by flow curvature and the presence of recirculation and is complex. The largest normal stresses are found just downstream of the trailing edge and decrease between here

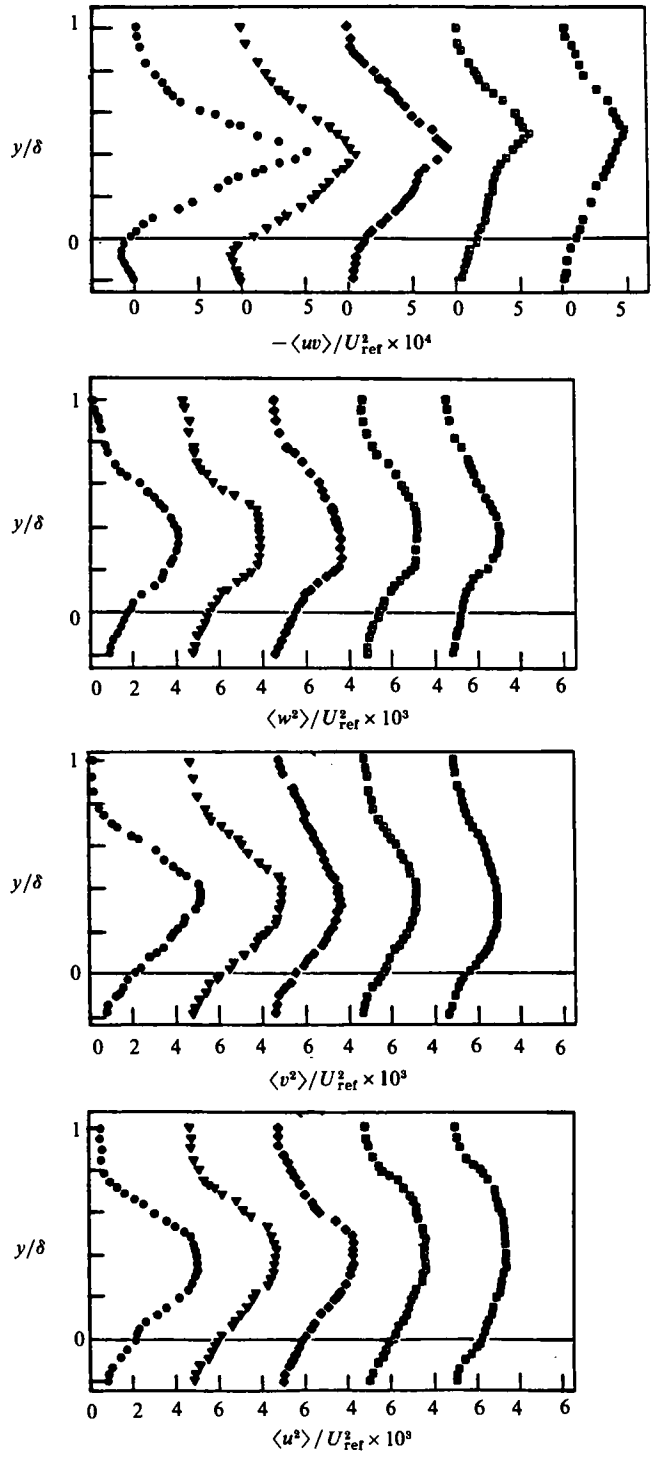

FIGURE 11. Distribution of Reynolds stresses in the far wake. (Symbols are as on figure 4(*c*) with the following addition: ⊕, $x/c = 0.824$.

and the location where instantaneous flow reversals are no longer found, which is at x/c of about 0.08. Farther downstream, the shear layers from the suction and pressure sides interact and stresses have two maxima located approximately at the inflection points in the mean-velocity distribution. The shear stress increases rapidly on the suction side from just upstream of the trailing edge and attains its largest value at x/c of 0.012. This behaviour is due to increased production and decreased dissipation associated with convergence and destabilizing curvature of the flow around the downstream end of the recirculating region. Turbulence diffusion is also important here and acts to make the normal stresses constant over about 20 % of the wake thickness in the vicinity of their maxima.

The second set of normal-stress maxima occurring in the pressure-side shear layer are smaller than those on the suction side. The pressure-side maxima in $\langle v^2 \rangle$ and $\langle w^2 \rangle$ increase rapidly over the very near wake and are almost equal to the larger maxima on the suction side at x/c of 0.10. The pressure-side $\langle u^2 \rangle$-maxima, however, remains almost constant with downstream distance although it moves towards the centre of the wake in conjunction with the inflection point in the mean-velocity profile. The values of $\langle w^2 \rangle$ change very rapidly at the downstream end of the very near wake and decrease by as much as 50 % over the last 50 mm. Here also, the distributions of $\langle u^2 \rangle$ and $\langle v^2 \rangle$ remain relatively constant in the lower shear layer but their values are substantially reduced near the suction-side maxima.

The Reynolds shear stress changes sign at the location of minimum mean velocity and is distributed differently along the suction-side and pressure-side shear layers. On the suction side, a local maximum value of $\langle uv \rangle$ exists just downstream of the trailing edge and decreases to its lowest value by the end of the very near wake. Smaller values of $\langle uv \rangle$ were measured in the lower shear layer and increase from their boundary-layer value at the trailing edge to a maximum of 2.1 m^2/s^2 at x/c of 0.10, which corresponds approximately to the location where the two shear layers collide.

Farther downstream, the maxima associated with the lower shear layer diminish with downstream distance and become indistinguishable beyond x/c of 0.26 although negative values of $\langle uv \rangle$ are found up to x/c of 0.41. In the near wake, between x/c of about 0.10 and 0.23, the normal stresses increase in the vicinity of the suction-side maxima although the opposite might be expected since the rate of their production is reduced because of decreasing gradients of streamwise and cross-stream mean velocity. The rate of dissipation is, however, significantly lowered because of the destabilizing curvature and the shear-stress production of normal stresses is large. The maxima in the normal-stress profiles increase at the downstream end of the near wake and before any significant change is apparent in the mean flow.

Turbulence decays in the far wake as the flow recovers to a plane mixing layer. A single maximum is observed in the profiles of all four Reynolds stresses of the far wake, and the relative magnitudes of the normal stresses were found to be

$$\langle u^2 \rangle > \langle v^2 \rangle > \langle w^2 \rangle, \tag{5}$$

which was also observed by Hah & Lakshminarayana (1982) in the asymmetric wake of an aerofoil with attached turbulent boundary layers leaving the trailing edge.

5. Discussion

It is evident from the results of the previous two sections that the influence of the separated-flow region is large, even though the details of the flow within this region may be relatively unimportant. Normal stresses and cross-stream pressure gradients

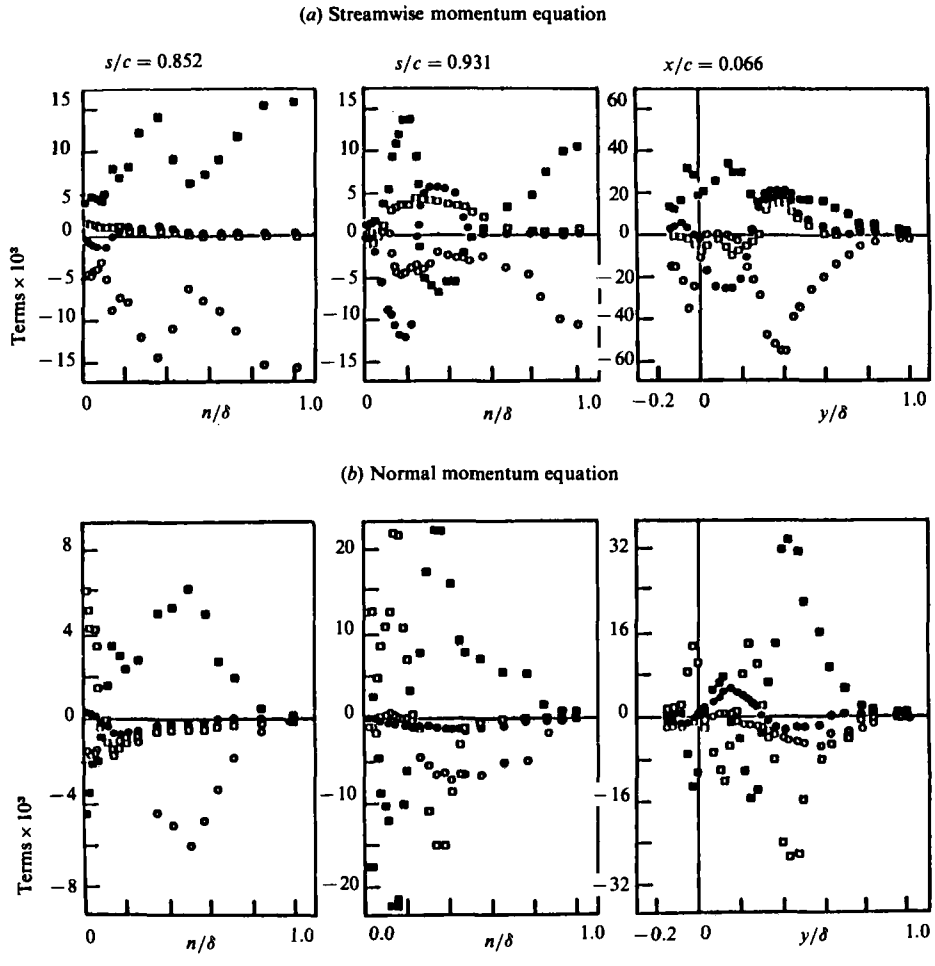

FIGURE 12. Terms in the momentum transport equations.

(*a*) ○, $\frac{\delta_1}{U_e^2}\left[\langle U\rangle\frac{\partial\langle U\rangle}{\partial x}+\langle V\rangle\frac{\partial\langle U\rangle}{\partial y}\right]$; □, $\frac{\sigma_1}{U_e^2}\frac{\partial\langle u^2\rangle}{\partial x}$;
●, $\frac{\delta_1}{U_e^2}\frac{\partial\langle uv\rangle}{\partial y}$; ■, $\frac{\delta_1}{U_e^2}\frac{\partial\langle P\rangle}{\partial x}$ imbalance.

(*b*) ○, $\frac{\delta_1}{U_e^2}\left[\langle U\rangle\frac{\partial\langle V\rangle}{\partial x}+\langle V\rangle\frac{\partial\langle V\rangle}{\partial y}\right]$; □, $\frac{\delta_1}{U_e^2}\frac{\partial\langle v^2\rangle}{\partial y}$;
●, $\frac{\delta_1}{U_e^2}\frac{\partial\langle uv\rangle}{\partial x}$; ■, $\frac{\delta_1}{U_e^2}\frac{\partial\langle P\rangle}{\partial y}$ imbalance.

play an important role immediately upstream and downstream of the recirculating flow and are associated with strong curvature of the streamlines. Figure 12 helps to put those effects into perspective by displaying terms which balance the U and V momentum-transport equations at locations which are immediately upstream, in and immediately downstream of the recirculating flow.

Immediately upstream of mean-flow separation, the pressure gradient and convective terms dominate with the components of the V-momentum equation tending

	Maximum values of the Reynolds stresses			
	$\frac{\langle u^2 \rangle}{\langle U_{ref} \rangle^2}$ ($\times 10^3$)	$\frac{\langle v^2 \rangle}{\langle U_{ref} \rangle^2}$ ($\times 10^3$)	$\frac{\langle w^2 \rangle}{\langle U_{ref} \rangle^2}$ ($\times 10^3$)	$\frac{\langle uv \rangle}{\langle U_{ref} \rangle^2}$ ($\times 10^3$)
Attached boundary layer just upstream of separation				
Simpson *et al.* (1981)	9.5	3.0	3.5	−1.8
Coles & Wadcock (1979)	20	10	—	−7.5
Present	3.7	1.6	1.9	−0.35
Separated region				
Simpson *et al.* (1981)	40	20	23	−6.0
Coles & Wadcock (1979)	85	55	—	−17.5
Present	10.2	6.3	10.0	−5.2
Wake region				
Coles & Wadcock (1981)	30	30	—	−7.5
Nakayama (1983)	30	13	—	−10.0
Present	9.0	5.0	5.0	−1.6

TABLE 2. Maximum values of Reynolds stresses and comparison with other experiments

in magnitude to those of the U-momentum equation as separation is approached. The effects of the turbulent structure are relatively unimportant in this upstream region and the same situation exists in the outer flow surrounding the region of negative velocities. This emphasis changes inside the recirculating flow, where the importance of the shear and normal stresses is greater. Turbulent diffusion, in particular, is important in the U-momentum equation and is almost in balance with the pressure gradient up to the location of zero mean velocity. The pressure-gradient term is of the same order of magnitude in the two equations and, in the V-momentum equation, tends to balance with the normal-stress term up to the location of zero mean velocity. Careful inspection of the upstream flow indicates that this trend is also present but confined to the very-near-wall region. In the near wake, the cross-stream pressure gradient dominates the flow with a maximum influence well outside the region of negative velocities. The normal stresses are at least as important as the shear stresses in the mean momentum balance.

The importance of the pressure-gradient terms in the momentum equations explains, in part, why design methods can sometimes escape without detailed consideration of turbulence phenomena. The importance of the V-momentum equation should, however, be noted and the varying magnitudes of the normal-stress and shear-stress terms clearly demonstrates that accurate representations of the flow cannot be achieved without their consideration.

It should be noted that the magnitude of the present crossflow pressure gradients is associated with the streamline curvature and the size of the region of recirculating flow. The smaller regions of separation, such as those present in the flows of Coles & Wadcock (1979) and Nakayama (1984), lead to smaller crossflow pressure gradients. On the other hand, the stabilizing effect of the curvature of the surface upstream of separation has resulted in smaller values of Reynolds stresses in the boundary layer immediately upstream of separation than found by Coles & Wadcock (1979), Simpson *et al.* (1981) and Nakayama (1984). The maximum values of Reynolds stresses for the flows of Coles & Wadcock, Simpson *et al.* and the present work are provided in table 2. In both respects, the various flows show consistent

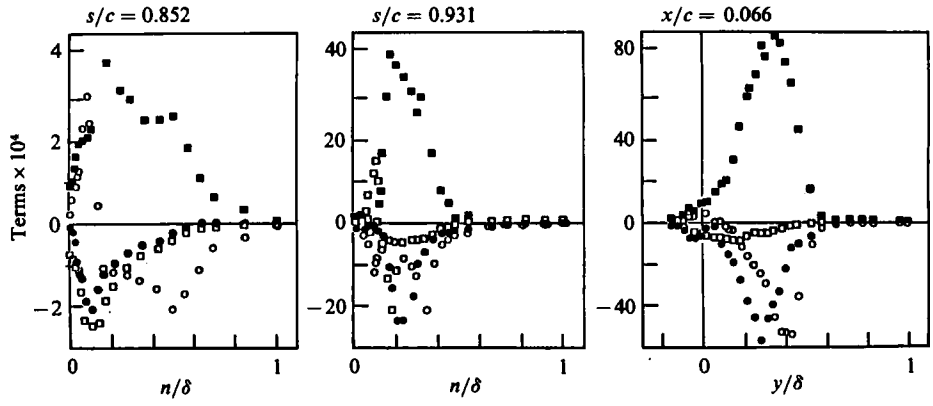

FIGURE 13. Terms in the transport equation for turbulence kinetic energy.

$$\bigcirc,\ \frac{\delta_1}{U_e^3}\left[\langle U\rangle\frac{\partial k}{\partial x}+\langle V\rangle\frac{\partial k}{\partial y}\right];\quad \square,\ \frac{\delta_1}{U_e^3}[\langle u^2\rangle-\langle v^2\rangle]\frac{\partial\langle U\rangle}{\partial x};$$

$$\bullet,\ \frac{\delta_1}{U_e^3}\langle uv\rangle\frac{\partial\langle U\rangle}{\partial y};\qquad \blacksquare,\ \text{imbalance.}$$

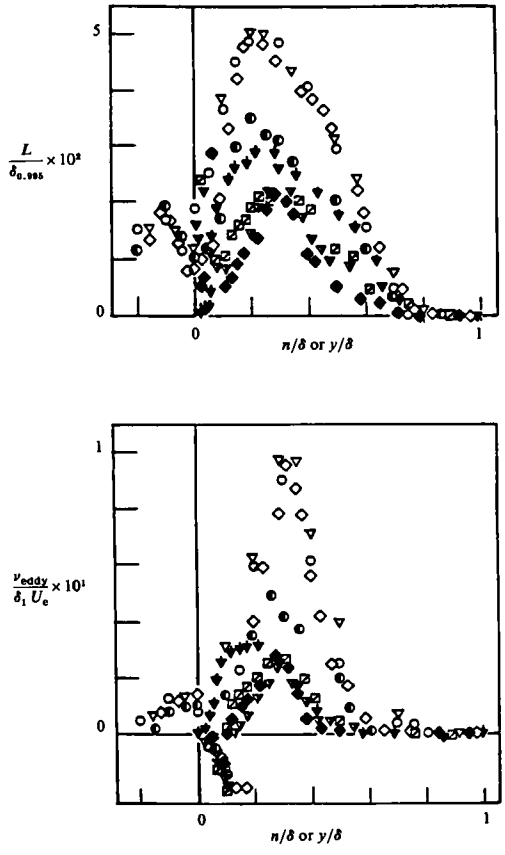

FIGURE 14. Profiles of mixing length and eddy viscosity. $L = |\langle uv\rangle|^{\frac{1}{2}}/\partial\langle U\rangle/\partial y$; $\nu_{\text{eddy}} = \langle uv\rangle/\partial\langle U\rangle/\partial y$: ▼, $s/c = 0.852$; □, 0·886; ▽, 0.932; ■, 0.994. ◐, $x/c = 0.006$; ◇, 0.050; ○, 0.0660; ▽, 0.099.

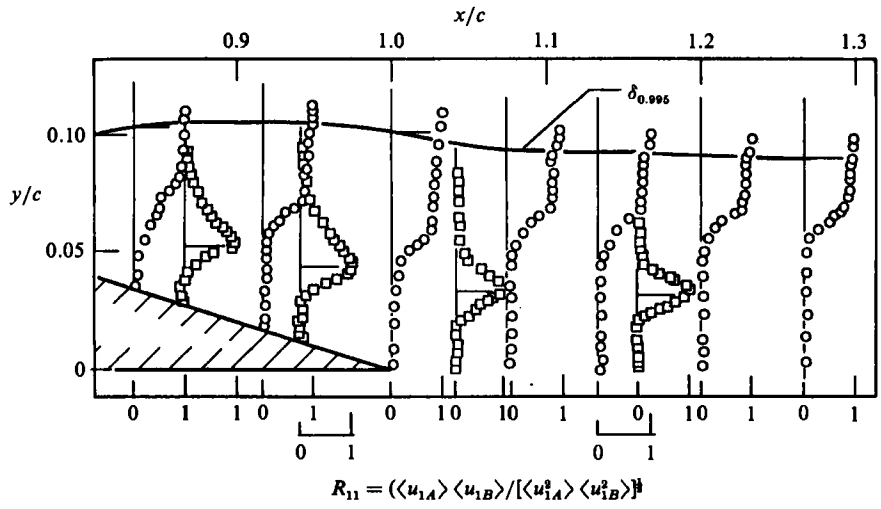

FIGURE 15. Distribution of the two-point correlation coefficient, R_{11}: ○, probe held at n/δ of y/δ of 1.1; □, probe held at n/δ or y/δ of 0.35.

trends but with important differences in magnitude. In the case of the Reynolds stresses, for example, the relative increases in the normal stresses $\langle u^2 \rangle$, $\langle v^2 \rangle$ and $\langle w^2 \rangle$ immediately upstream of separation are approximately 4, 5 and 6 for all flows. These values affect the stresses within the recirculating-flow region so that, in the present case, they are correspondingly lower.

The components of the turbulence-energy equation are shown on figure 13 and demonstrate clearly that the flow is far from equilibrium except in the upstream region and very close to the wall. Shear-stress and normal-stress production are important, with the latter having the greater influence in some regions, especially immediately upstream of mean-flow separation.

These general features of the flow suggest that design procedures which do not involve the cross-stream pressure gradient must fail and that simple turbulence assumptions will lead to the representation of approximate trends of mean-flow characteristics. Figure 14 presents values of mixing length and eddy viscosity and demonstrates their wide variations with position. In the near-wall region, the simple approach consistent with the law of the wall is increasingly less satisfactory as separation is approached and it is clear, though perhaps of secondary importance, that regions of logarithmic velocity do exist, although with varying slopes, in an around separation.

In support of interaction theory, though more of interaction between potential flow and viscous flow represented by the Navier–Stokes equations, figure 15 presents two-point correlation which show that the influence of the separated flow diminishes rapidly with y.

This work was supported by a grant from the Science and Energy Research Council. Thanks are due to D. Adair for his assistance in the latter stages of this experimental programme and to J. Laker and O. Vis for their continuing help with electronic and mechanical components.

REFERENCES

ADAIR, D., THOMPSON, B. E. & WHITELAW, J. H. 1984 Measurements and calculations of a separating boundary layer and the downstream wake. *Numerical and Physical Aspects of Aerodynamic Flows II* (ed. T. Cebeci), p. 97. Springer-Verlag.

CEBECI, T., STEWARTSON, K. & WHITELAW, J. H. 1984 Calculation of two-dimensional flow past airfoils. *Numerical and Physical Aspects of Aerodynamic Flows II* (ed. T. Cebeci), p. 1. Springer-Verlag.

COLE, D. E. & WADCOCK, A. J. 1979 Flying-hot-wire study of flow past an NACA 4412 airfoil at maximum lift. *AIAA J* **17**, 321.

GILLIS, J. C. & JOHNSTON, J. P. 1983 Turbulent boundary-layer flow and structure on a convex wall and its development on a flat wall. *J. Fluid Mech.* **135**, 123.

HAH, C. & LAKSHMINARAYANA, B. 1982 Measurement and prediction of mean velocity and turbulence structure in the near wake of an airfoil. *J. Fluid Mech.* **115**, 251.

HASTINGS, R. C. & MORETON, K. G. 1982 An investigation of a separating equilibrium turbulent boundary layer. *Proc. Intl Sym. Applications of Laser-Doppler Anemometry to Fluid Mech. Lisbon, Portugal.* Paper 11.

HOFFMAN, P. H. & BRADSHAW, P. 1978 Turbulent boundary layers on surfaces of mild longitudinal curvature. *Imp. College Aero Report* 78-04.

MCDONALD, H. & BRILEY, W. R. 1984 A survey of recent work on interacted boundary-layer theory for flow with separation. *Numerical and Physical Aspects of Aerodynamic Flows II* (ed. T. Cebeci), p. 141. Springer-Verlag.

NAKAYAMA, A. 1984 Measurements of attached and separated turbulent flows in the trailing-edge region of airfoils. *Numerical and Physical Aspects of Aerodynamic Flows II* (ed. T. Cebeci), p. 233. Springer-Verlag.

SIMPSON, R. J., CHEW, Y. T. & SIVAPRASAD, B. G. P. 1981 The structure of a separating turbulent boundary layer. *J. Fluid Mech.* **113**, 23.

SO, R. M. C. & MELLOR, G. L. 1973 Experiment on convex curvature effects in turbulent boundary layers. *J. Fluid Mech.* **60**, 43.

THOMPSON, B. E. 1984 The turbulent separating boundary layer and downstream wake. Ph.D. Thesis, University of London.

THOMPSON, B. E. & WHITELAW, J. H. 1982 A turbulent boundary layer approaching separation. *Walz-Festschrift Volume*, p. 253. Springer-Verlag.

THOMPSON, B. E. & WHITELAW, J. H. 1984 Flying hot-wire anemometry. *Exp. in Fluids* **2**, 47.

VISWANATH, P. R. & BROWN, J. L. 1983 Separating trailing-edge flow at a transonic Mach number. *AIAA J.* **21**, 801.